Heme Coordination States of Unfolded Ferrous Cytochrome *c*

Enrica Droghetti,* Silke Oellerich,† Peter Hildebrandt,† and Giulietta Smulevich*
*Dipartimento di Chimica, Università di Firenze, Sesto Fiorentino (FI), Italy; and †Technische Universität Berlin, Institut für Chemie, Berlin, Germany

ABSTRACT The structural changes of ferrous Cyt-*c* that are induced by binding to SDS micelles, phospholipid vesicles, DeTAB, and GuHCl as well as by high temperatures and changes in the pH have been studied by RR and UV-Vis absorption spectroscopies. Four species have been identified in which the native methionine-80 ligand is removed from the heme iron. This coordination site is either occupied by a histidine (His-33 or His-26) to form a 6cLS configuration, which is the prevailing species in GuHCl at pH 7.0 and ambient temperature, or remains vacant to yield a 5cHS configuration. The three identified 5cHS species differ with respect to the hydrogen-bond interactions of the proximal histidine ligand (His-18) and include a nonhydrogen-bonded, a hydrogen-bonded, and a deprotonated imidazole ring. These structural motifs have been found irrespective of the unfolding conditions used. An unambiguous spectroscopic distinction of these 5cHS species is possible on the basis of the Fe-N(imidazole) stretching vibrations, the RR bands in the region between 1300 and 1650 cm^{-1}, and the electronic transitions in the Soret- and Q-band regions. In acid and neutral solutions, the species with a hydrogen-bonded and a nonhydrogen-bonded His-18 prevail, whereas in alkaline solutions a configuration with a deprotonated His-18 ligand is also observed. Upon lowering the pH or increasing the temperature in GuHCl solutions, the structure on the proximal side of the heme is perturbed, resulting in a loss of the hydrogen-bond interactions of the His-18 ligand. Conversely, the hydrogen-bonded His-18 of ferrous Cyt-*c* is stabilized by electrostatic interactions which increase in strength from phospholipid vesicles to SDS micelles. The results here suggest that unfolding of Cyt-*c* is initiated by the rupture of the Fe-Met-80 bond and structural reorganizations on the distal side of the heme pocket, whereas the proximal part is only affected in a later stage of the denaturation process.

INTRODUCTION

Cyt-*c* is a small single domain heme protein which serves as an electron shuttle in the respiratory chain of aerobic organisms (1). Moreover, it has been recently discovered that it plays a role in programmed cell death (apoptosis) (2,3). The heme group is covalently bound to the polypeptide chain and coordinated by His-18 and Met-80 to yield a 6cLS configuration. The three-dimensional structure of Cyt-*c* has been well characterized by x-ray crystallography and NMR spectroscopy (4–6).

The importance of the natural function of this protein has stimulated numerous studies on its structure and dynamics. Furthermore, Cyt-*c* serves as a model protein for investigating fundamental folding and unfolding processes of polypeptide chains, and the impact of these studies goes far beyond the specific function of Cyt-*c*. Although the unfolding process of ferric Cyt-*c* in solution has been extensively explored (7–15), little is known about the folding and unfolding pathways of the reduced form, which is distinctly more resistant to denaturation than the ferric form (15–22, and references therein). The Fe-ligand bonds of ferrous Cyt-*c* are preserved over a wide range of temperatures and denaturant concentrations and, even in 9 M urea at neutral pH, the ferrous protein maintains its native structure. Equilibrium and kinetic studies of ferrous Cyt-*c* in GuHCl solution indicate that at neutral pH a 5cHS form coexists with a nonnative 6cLS heme and that the ratio of these two species is affected by the pH (13,23–26). In addition, UV-Vis absorption and NMR spectroscopies have revealed that at neutral pH SDS also induces a spin state change (14,27). RR spectroscopy (13) has shown that the latter corresponds to formation of two different 5cHS forms, both having the His-18 residue bound to the iron atom.

The previous studies on ferrous Cyt-*c* indicate that, in a similar manner to the ferric form, the unfolding/folding process of the protein includes various metastable states that exhibit a specific coordination state of the heme group. However, details of the respective heme pocket structures are not known. In this work we have employed UV-Vis absorption and RR spectroscopies to gain further insight into molecular interactions of the heme group in the various states that are formed during unfolding processes. In particular, we focused on identifying structural motifs of the unfolded species induced by different agents and external stimuli including extreme pH and temperatures and interactions with denaturants, SDS micelles, and phospholipid vesicles.

Submitted December 27, 2005, and accepted for publication July 6, 2006.

Address reprint requests to Giulietta Smulevich, Tel.: 39-055-4573083; Fax: 39-055-4573077; E-mail: giulietta.smulevich@unifi.it.

Silke Oellerich's present address is Experimental Physics IV, Universität Bayreuth, Universitätsstrasse 30, D-95447 Bayreuth, Germany.

Cyt-*c*, cytochrome *c*; MP8, microperoxidase-8; MP11, microperoxidase-11; GuHCl, guanidine hydrochloride; SDS, sodium dodecyl sulphate; DOPG, dioleoylphosphatidylglycerol; DeTAB, decyltrimethylammonium bromide; MES, 2-morpholinoethanesulfonic acid; cmc, critical micellar concentration; L/P, lipid/protein ratio; RR, resonance Raman; CCD, charge-coupled device; D^2, second derivative; 6cLS, six-coordinated low-spin; 5cHS, five-coordinated high-spin; 6cHS, six-coordinated high-spin; ν(Fe-Im), Fe-Im stretching mode; UV-Vis, ultraviolet-visible.

0006-3495/06/10/3022/10 $2.00

doi: 10.1529/biophysj.105.079749

MATERIALS AND METHODS

Materials

Horse heart Cyt-*c* (type VI) was purchased from Sigma-Aldrich (St Louis, MO). For quantitative studies, the protein was purified as previously described (28). MP11 was prepared following the procedures described by Wang et al. (29). Sample concentration was ~10–60 μM for RR spectroscopy. The UV-Vis absorption spectra of Cyt-*c* and MP11 were obtained with a concentration of 5–50 and 50–150 μM, respectively. Buffers for pH 5.0, 6.0, and 7.0 were 100 mM acetate, MES, and HEPES, respectively. For experiments with DOPG liposomes, a pH value of 7.0 was established by 5 mM HEPES/1 mM EDTA buffer; 9 M urea, 6.3 M GuHCl, and 75 mM SDS solutions were prepared with 50–100 mM buffer at the desired pH. For highly alkaline solutions, DeTAB was dissolved in 2.5 M NaOH to yield a DeTAB concentration of 300 mM. DeTAB, purchased from Fluka Chemie (Buchs, Switzerland), was recrystallized twice from acetone. Solutions of unfolded polypeptide were prepared by dissolving Cyt-*c* and MP11 in denaturant stock solutions.

Deuterated ferric Cyt-*c* and MP11 in SDS or DeTAB were prepared at neutral and alkaline pD, respectively. The protein was then reduced by sodium dithionite in D_2O (99.9%) (Merck KGaA, Darmstadt, Germany) as described below. No spectral variations were observed with respect to the H_2O buffers—either for Cyt-*c* or for MP11.

The ferrous forms were obtained by addition of a few microliters of a freshly prepared sodium dithionite solution (10 mg/ml) to the deoxygenated fresh polypeptide solution. The heme coordination state of the ferrous protein in GuHCl was found to be dependent on the concentration of the reducing agent. A high amount of sodium dithionite (>60:1 dithionite/protein molar ratio) gave rise to the formation of a new 6cLS heme, irrespective of the pH value (see Supplementary Material). The formation of this species was also observed at lower sodium dithionite concentration when the protein had spent more than 2 h in the denaturant solution before reduction. Thus, reduction of Cyt-*c* in the presence of GuHCl was achieved with the smallest amount of sodium dithionite required to fully reduce the protein (from dithionite/Cyt-*c* molar ratios of 40:1 at pH 7.0 to 100:1 at pH 4.8). Furthermore, each spectrum was recorded using a freshly prepared sample.

Thermal denaturation was performed in thermostated cuvettes by progressively raising the temperature from 20°C to 95°C. The spectra of Cyt-*c* were recorded after the solution had reached thermal equilibrium by keeping the sample at the desired temperature for ~1 min. The rate of heating between the set temperatures was ~3°C min^{-1}.

DOPG was purchased from Sigma. Dry films of 10 mg lipid were prepared from a stock solution in chloroform under a nitrogen stream and left under vacuum for at least 8 h to remove all traces of the organic solvent. The lipid films were resuspended in HEPES/EDTA buffer and gently vortexed for a few minutes. Large unilamellar vesicles with a diameter of ~150 nm were then prepared by sequential extrusion through polycarbonate membranes (Avanti Lipids) of decreasing pore size diameter. Vesicle sizes and their distribution as well as vesicle stability were checked by dynamic light scattering using an ALV goniometer system with fiber optic detection.

Methods

Electronic absorption and RR spectra were collected at room temperature unless specified otherwise. Electronic absorption spectra, measured with a double-beam Cary 5 spectrophotometer (Varian, Palo Alto, CA), were recorded both before and after the RR measurements. No sample degradation was observed under the experimental conditions employed.

D^2 spectra (LabCalc, Galactic Industries, Salem, NH) were obtained using the Savitzky-Golay method with 15 data points. No changes in the wavelength or in the bandwidth were observed when the number of points was increased or decreased.

RR spectra were measured with 413.1 nm (Kr^+ laser, Coherent, Innova 300 C, Santa Clara, CA), 476.5-nm (Ar^+ laser, Coherent, Innova 90/5), and 441.6-nm excitation (He-Cd laser, Kimmon IK4121R-G, Tokyo, Japan). Except for the quantitative analysis, the RR spectra were recorded using samples in slowly rotating NMR tubes (backscattering) and either a double monochromator (Jobin-Yvon HG2S, Villeneuve d'Ascq, France) equipped with a cooled photomultiplier (RCA C31034A, Burle Industries GmbH, Baesweiler, Germany) and photon-counting electronics, or a triple spectrometer (consisting of two Acton Research SpectraPro2300i and a SpectraPro 2500i in the final stage with a 1800 grooves/mm grating) (Acton, MA) working in a subtractive mode, equipped with a liquid nitrogen cooled CCD detector (Roper Scientific Princeton Instruments, Trenton, NJ) were used.

RR spectra used for the quantitative analysis were measured using samples in rotating quartz cells (90° scattering) and a double monochromator operated as a spectrograph and equipped with a liquid-nitrogen cooled CCD detector (U1000, ISA). In these experiments the spectral resolution was 4 cm^{-1} with a wavenumber increment per data point of 0.53 cm^{-1}. Details of the experimental setup are given elsewhere (13).

All RR measurements were repeated several times under the same conditions to ensure reproducibility. To improve the signal/noise ratio, a number of spectra were accumulated and summed only if no spectral differences were noted. The RR spectra were calibrated with indene and CCl_4 as standards to an accuracy of 1 cm^{-1} for intense isolated bands. The relative intensities of the high-frequency RR spectra in the figures are normalized on the ν_4 band. Before the spectra analysis contributions from the unfolding agents and the structureless background were subtracted. For the quantitative determination of the individual species, a component analysis was applied to the RR spectra in the high-frequency region (1300–1650 cm^{-1}) as described previously (13,30). The spectral region between 150 and 300 cm^{-1} was analyzed by a band-fitting program (Lab Calc) restricting the number of bands to the number of peaks and shoulders detectable in the original spectrum (see Supplementary Material). The reliability of the fits was checked by analyzing spectra obtained with different excitation lines but under otherwise identical conditions. Thus, only relative band intensities were allowed to vary, whereas frequencies and halfwidths were fixed.

RESULTS AND DISCUSSION

Different states of unfolded ferrous Cyt-*c* and microperoxidases

Detergent binding

The electronic absorption spectrum of ferrous Cyt-*c* in buffer solution at pH 7.0 displays a Soret band at 415 nm and Q bands at 520 and 550 nm, which are typical of a 6cLS heme with a Met/His coordination (31). Upon binding to SDS above the cmc, the UV-Vis spectrum of Cyt-*c* is drastically altered with broad Soret and Q bands at 422 and 550 nm, respectively (Fig. 1 *A*) (14). The spectrum is very similar to that of the mono-His ligated Cyt-*c*′ at pH 8.0 (32) and of microperoxidases MP8 (33) and MP11 in SDS (Fig. 1 *A*). MP8 and MP11 are the products of proteolytic digestion of Cyt-*c*, containing the proximal His-18 ligand as a part of a residual 8- and 11-membered peptide, containing the amino acid sequence 14–21 and 11–21 of Cyt-*c*, respectively (34). The D^2 spectra of Cyt-*c* and MP11 reveal more clearly the shoulders on the long wavelength side of the Soret and Q bands (at 433 and 565 nm). These bands indicate the coexistence of (at least) two different species. In addition, the RR spectra in the spin state marker band region (1300–1650 cm^{-1}) of reduced MP11 and Cyt-*c* in SDS at pH 7.0 are quite similar and characteristic of a 5cHS heme with bands at 1353

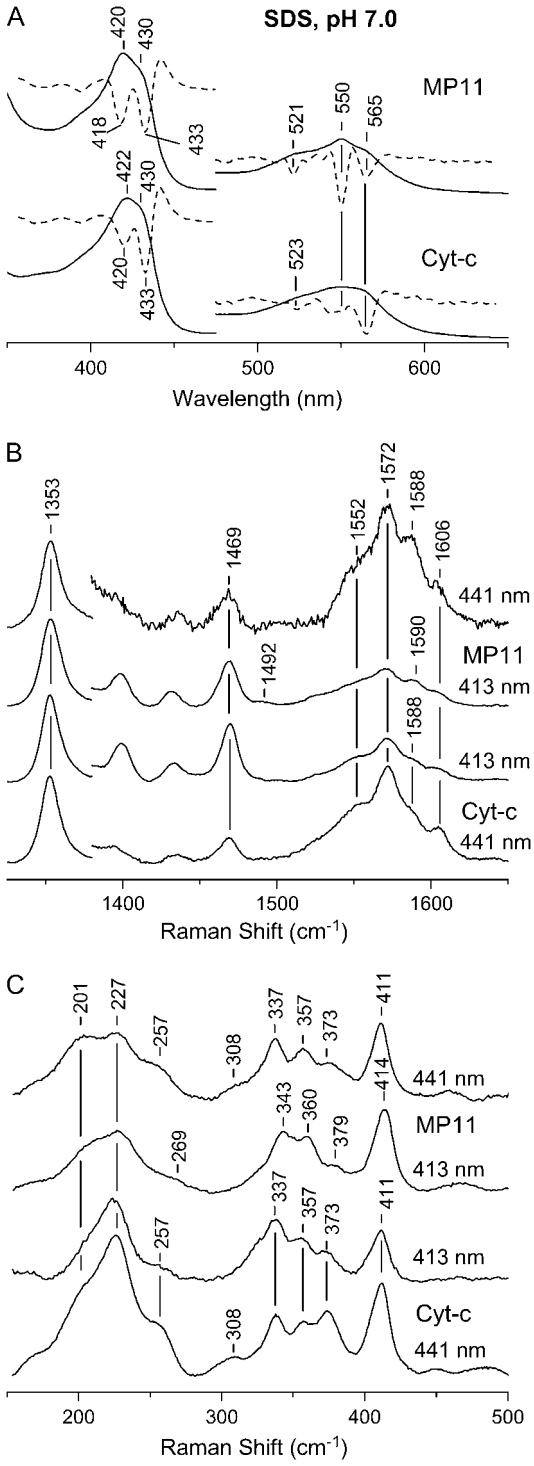

FIGURE 1 (*A*) Electronic absorption and D^2 (*dotted line*) spectra of ferrous MP11 (*upper trace*) and Cyt-*c* (*lower trace*) in 75 mM SDS at pH 7.0, and RR spectra measured in the marker band (*B*) and low-frequency region (*C*), using 413- and 441-nm excitations. The 475–650 nm region in the absorption spectrum (*A*) has been expanded by a factor of three. The RR spectra (*B*,*C*) were measured with a laser power of 10–20 mW at the sample, a spectral resolution of 4 cm^{-1} (413 nm) and 3 cm^{-1} (441 nm), and integration times between 5 and 150 min. The 1380–1650 cm^{-1} and 150–500 cm^{-1} regions have been expanded by a factor of three and seven, respectively.

(ν_4), 1469 (ν_3), 1552 (ν_{11}), 1572 (ν_2), 1588 (ν_{37}), and 1606 cm^{-1}(ν_{10}) (Fig. 1 *B*). However, MP11 also includes a small contribution of a 6cLS form as reflected by the weak band at 1492 cm^{-1} (ν_3) (35). This 6cLS species appears to be formed at the expense of the minor 5cHS species characterized by the 430- and 565-nm bands (Fig. 1 *A*). However, the contribution of the 6cLS species is too low to allow the identification of the respective bands in the UV-Vis absorption spectrum.

A band-fitting analysis of the RR marker bands of Cyt-*c* in SDS reveals two 5cHS species with the ν_4 modes at 1353.7 and 1359.9 cm^{-1} for the dominant and minor forms, respectively (13). These two forms, which have also been identified upon binding to DOPG vesicles (Supplementary Material), have been attributed to hemes with different hydrogen-bonding interactions of the His-18 ligand (13). Since the ν_4 mode is a sensitive indicator of the electron density on the porphyrin, a downshift of its frequency to 1353 cm^{-1} has been related to an increase of the electron-donating capability of the axial ligand, which can be in turn a consequence of stronger hydrogen-bond interactions of the $N_\delta H$ group of the imidazole ring. In contrast to this species, denoted as [5cHS(1)], the ν_4 mode at 1360 cm^{-1} corresponds to a heme with a ''normal'' electron density on the porphyrin [5cHS(2)], ruling out significant hydrogen-bond interactions of the His-18 ligand.

Since these 5cHS species should differ with respect to the interactions of the histidine ligand, it is instructive to analyze the iron-imidazole stretching ν(Fe-Im), which is expected to give rise to a strong band in the region between 200 and 250 cm^{-1} upon Soret excitation (36). In fact, studies of model 5-coordinated ferrous porphyrins have demonstrated that the Fe-Im stretching frequency is a sensitive indicator of the status of the hydrogen-bond interactions of the coordinated imidazole (37,38).

The low-frequency RR spectrum of Cyt-*c* in SDS obtained with 441-nm excitation, i.e., in resonance with the maximum at ~430 nm (Fig. 1 *A*), displays a strong band at 227 cm^{-1} with shoulders at 201 cm^{-1} and 257 cm^{-1} (Fig. 1 *C*). The band at 227 cm^{-1}, which is not found in the RR spectrum of the native form of ferrous Cyt-*c* (39), decreases in intensity upon 413-nm excitation, i.e., in resonance with the Soret maximum at 422 nm, since the ν(Fe-Im) mode is strongly coupled to the Soret resonance (36). In the spectrum obtained with 476-nm excitation (spectrum not shown) both bands at 201 and 227 cm^{-1} almost disappear. These intensity changes, as a function of the excitation wavelength, allow the assignment of the 227 cm^{-1} band to the ν(Fe-Im) mode of the 5cHS(1) species with the Soret maximum at 430 nm.

The relatively high frequency of 227 cm^{-1}, which is identical to that found for the 1–57 N-fragment of Cyt-*c* (40) and for Cyt-*c*′ (41), is reminiscent of the frequencies observed for those peroxidases in which a hydrogen-bond is formed between the $N_\delta H$ proton of the imidazole ring and an Asp residue (42). In Cyt-*c*, the side-chain carbonyl oxygen atom of Pro-30, which is located at 2.7 Å from the N_δ of the imidazole (43), is a possible candidate for a hydrogen-bond accepting

group (see Santoni et al. (40) for an illustrative figure). However, it is also possible that other hydrogen-bond acceptors are in close proximity to His-18 as a consequence of the SDS-induced structural changes of the protein (vide infra). An alternative explanation of the high Fe-Im stretching frequency, based on reduced repulsive interactions between the histidine ligand and the pyrrole nitrogens (44), is considered to be less likely as it cannot account for a substantial increase in the electron density of the porphyrin, as reflected by the low ν_4 mode frequency (13).

The second Fe-Im stretching at 201 cm^{-1}, attributed to the [5cHS(2)] form, is indicative of a weakly hydrogen-bonded histidine, which again is in agreement with the conclusions drawn from the frequency of the corresponding electron density marker band ν_4.

Two ν(Fe-Im) modes at 201 and 227 cm^{-1} are also found in the RR spectrum of MP11, and bands at very similar positions have been previously reported for MP8 in SDS at pH 7.0 (33). Based on the amino acid sequence of the undecapeptide MP11 (34), we propose that the strongly hydrogen-bonded His (227 cm^{-1}) results from the interaction of $N_\delta H$ group with Glu21, whereas the weakly hydrogen-bonded His (201 cm^{-1}) is attributed to the interactions with the solvent (water). Othman et al. (33) have further shown that in alkaline solutions of cetyltrimethylammonium bromide these bands are replaced by a new band at 243 cm^{-1} which, hence, was attributed to the stretching mode involving a deprotonated His-18. The unfolded forms of Cyt-*c* and MP11 in DeTAB in very alkaline solutions display an intense band at 251 cm^{-1} (441-nm excitation) (Fig. 2 *C*), which disappears upon 413-nm excitation. This band is assigned to Fe-Im stretching involving a deprotonated His ligand. This rather high frequency is nearly identical to that found for peroxidases, which also possess a deprotonated histidine ligand (42). The weak shoulder at 213 cm^{-1} (see Supplementary Material), which only slightly decreases upon 413-nm excitation, is assigned to the ν_{53} mode of the porphyrin as in the native Cyt-*c* (39).

The corresponding RR spectra in the marker band region (Fig. 2 *B*) largely reflect a 5cHS form, although a small contribution from a 6cLS heme can be detected (ν_3 and ν_2 at 1492 and 1591 cm^{-1}, respectively) (35). This unfolded ferrous Cyt-*c* species, possessing a deprotonated His ligand, is denoted [5cHS(3)].

Both the unfolded ferrous Cyt-*c* and MP11 in alkaline solutions show similar maxima and minima (420, 437, 522, 551, 565, and 586 nm) in the D^2 spectra, albeit with different relative intensities (Fig. 2 *A*). In particular, the intensity ratio of the bands in the Soret region appears to be reversed in Cyt-*c* as compared to MP11. Moreover, the minimum at 420 nm observed in the D^2 spectrum of Cyt-*c* is relatively broad.

Cyt-c binding to phospholipid vesicles

Binding of ferrous Cyt-*c* to DOPG vesicles at high L/P ratios and to SDS micelles is associated with similar spectral

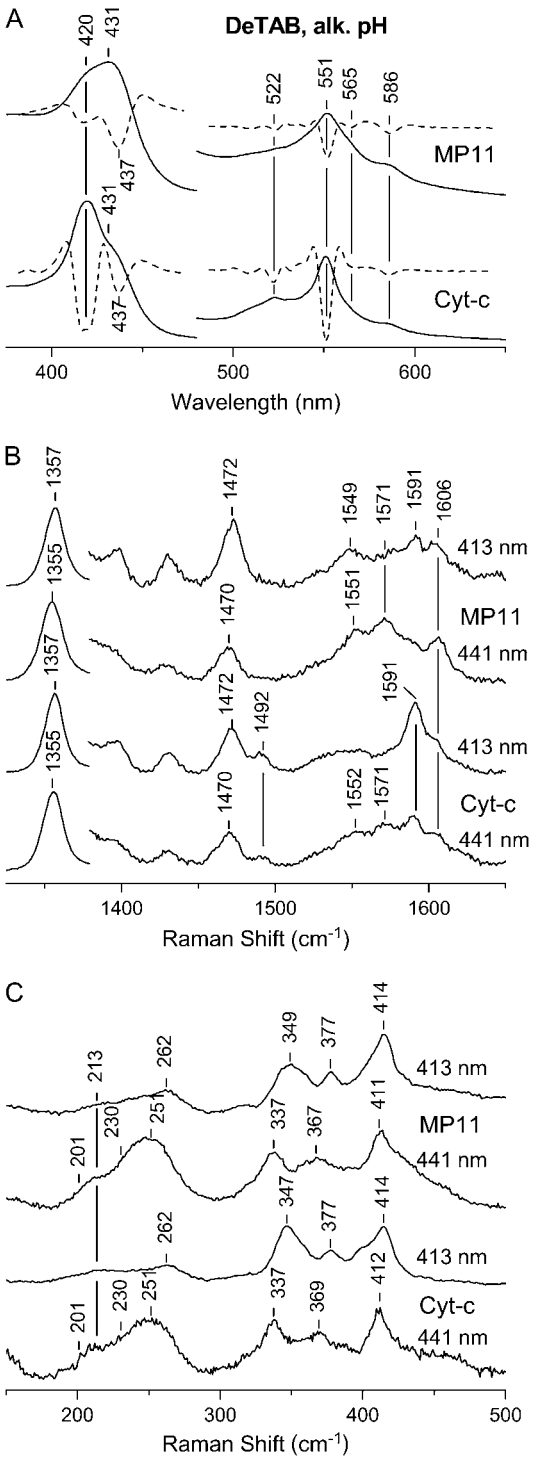

FIGURE 2 (*A*) Electronic absorption and D^2 (*dotted line*) spectra of ferrous MP11 (*upper trace*) and Cyt-*c* (*lower trace*) in 300 mM DeTAB at alkaline pH (2.5 M NaOH), and RR spectra measured in the marker band (*B*) and low-frequency region (*C*), using 413- and 441-nm excitations. The 480–650 nm region in the absorption spectrum (*A*) has been expanded by a factor of three. The RR spectra (*B*,*C*) were measured with a laser power of 10 mW at the sample, a spectral resolution of 4 cm^{-1} (413 nm) and 3 cm^{-1} (441 nm), and integration times between 10 and 70 min. The 1380–1650 cm^{-1} and 150–500 cm^{-1} regions have been expanded by a factor of five and seven, respectively.

changes. The UV-Vis and D^2 spectra (Fig. 3 *A*) reflect the contributions of both the 5cHS(1) and 5cHS(2) forms albeit with different relative contributions, as judged by the relative intensities of the Soret bands at 417 and 427 nm. Moreover, the spectra appear very similar to those recorded for MP11 in SDS, suggesting the presence of a small amount of a 6cLS heme coexisting with the HS species. These conclusions are confirmed by the RR spectra (Fig. 3, *B* and *C*). In the high-frequency region (Fig. 3 *B*), a small amount of a 6cLS form is reflected by the weak band at 1492 cm^{-1} (ν_3), which coexists with the 5cHS species. Moreover, the positions of the ν_4 marker bands in the RR spectra obtained with different excitations reflect the coexistence of both 5cHS(1) and 5cHS(2) forms, which again is consistent with the UV-Vis absorption data. Finally, in the low-frequency region (Fig. 3 *C*) two ν(Fe-Im) modes are observed at 201 and 227 cm^{-1}, which are very intense upon 441-nm excitation but disappear for 413-nm excitation.

Guanidinium hydrochloride denaturation

In neutral GuHCl solution the absorption bands broaden and the maxima shift to longer wavelengths with respect to native Cyt-*c* (Fig. 4) as reported previously (13,17,23,24). Specifically, in the D^2 spectra we note minima at ~417, 520, and 550 nm attributed to a nonnative 6cLS heme, together with a weak shoulder at ~430 nm originating from the 5cHS species. Upon increasing the temperature to 95°C or lowering the pH, the Soret band slightly shifts to longer wavelengths and the visible region further broadens although the band structure is better resolved as compared to ferrous Cyt-*c* in SDS (Fig. 4). The intensity of the 430-nm band increases and appears to include contributions from both [5cHS(2)] and [5cHS(1)], for which the respective maxima have been found at 422 and 430 nm for Cyt-*c* in SDS.

The RR spectra in the high-frequency region recorded in resonance with both Soret bands confirm the presence of both 5cHS and a 6cLS forms (Fig. 5). At neutral pH the prevailing form is a 6cLS heme, although the spectral features of a 5cHS heme can be detected. Upon heating the sample or lowering the pH the HS heme dominates. The positions of the ν_4 marker bands reflect the coexistence of both 5cHS forms, which again is consistent with the UV-Vis absorption data.

In the low-frequency region (Fig. 5) at pH 7.0, a band at 227 cm^{-1} is observed, which is relatively intense for 441-nm excitation but markedly decreases with 413-nm excitation. Upon heating the sample or lowering the pH from 7.0 to 5.0 a new band at 201 cm^{-1} is observed. The intensity of this band is comparable to that at 227 cm^{-1} in the spectrum obtained at 95°C, whereas it increases at pH 5.0. Both bands exhibit a lower intensity in the RR spectrum obtained with 413-nm excitation. The bands at 201 and 227 cm^{-1} are, therefore, assigned to the ν(Fe-Im) stretching modes of the 5cHS(2) and 5cHS(1) species, respectively.

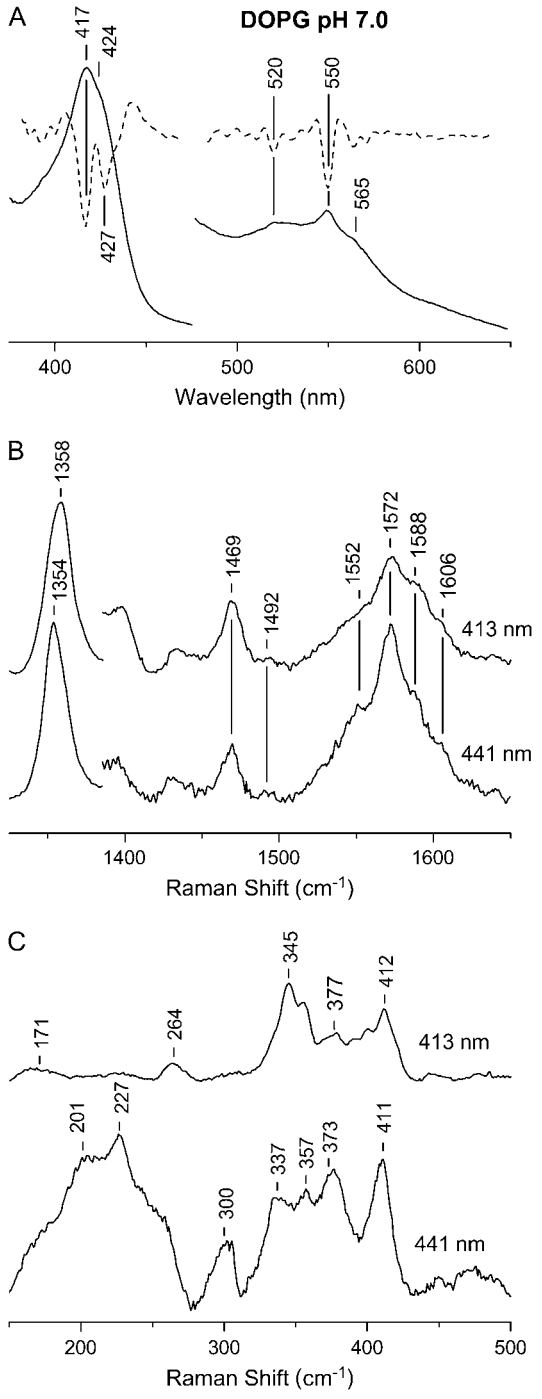

FIGURE 3 (*A*) Electronic absorption and D^2 (*dotted line*) spectra of Cyt-*c* in DOPG 5 mM (1:100) at pH 7.0, and RR spectra measured in the marker band (*B*) and low-frequency region (*C*), using 413- and 441-nm excitations. The 475–650 nm region in the absorption spectrum (*A*) has been expanded by a factor of three. The RR spectra (*B*,*C*) were measured with a laser power of 10 mW at the sample, a spectral resolution of 4 cm^{-1} (413 nm) and 3 cm^{-1} (441 nm), and integration times between 10 and 130 min. The 1385–1650 cm^{-1} and 150–500 cm^{-1} regions have been expanded by a factor of three and seven, respectively.

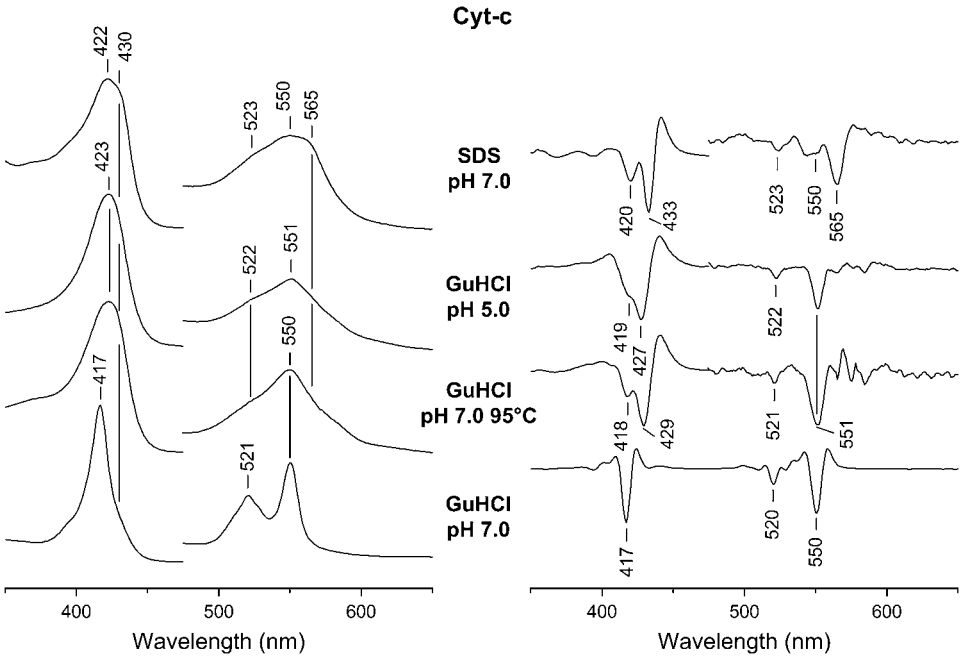

FIGURE 4 Electronic absorption spectra (*left panel*) and D^2 spectra (*right panel*) of ferrous Cyt-*c*. From top to bottom: SDS (75 mM, pH 7.0); GuHCl (6.3 M, pH 5.0); GuHCl (6.3 M, pH 7.0, 95°C); GuHCl (6.3 M, pH 7.0). The 475–650 nm region has been expanded by a factor of five.

Nonnative states of ferrous Cyt-c

The UV-Vis absorption and RR spectroscopic results demonstrate that there are (at least) four nonnative states of ferrous Cyt-*c* that exhibit specific structural properties of the heme pocket. These states include a 6cLS and three 5cHS species. The 5cHS species lack the Met-80 ligand and differ with respect to the location of the N(δ) proton of the imidazole ring of the proximal His-18 ligand. The 6cLS species should correspond to a heme in which the Met-80 ligand is replaced by a His ligand. In fact, under similar conditions, ferric Cyt-*c* forms a bis-His ligated 6cLS state with His-33 (or His-26) serving as the sixth ligand (13,15 and references therein). This ferric bis-His ligated Cyt-*c* has been found both in the presence of denaturing agents and upon binding to electrostatic or hydrophobic surfaces.

The techniques employed in this study are not sensitive to structural changes induced in the protein matrix. Thus, each of the four heme configurations identified in this work may be associated with different protein structures, which depend on the ''unfolding'' conditions by which they are produced. The minimum structural change that is required for the formation of the 5cHS species is the rupture of the Fe-Met-80

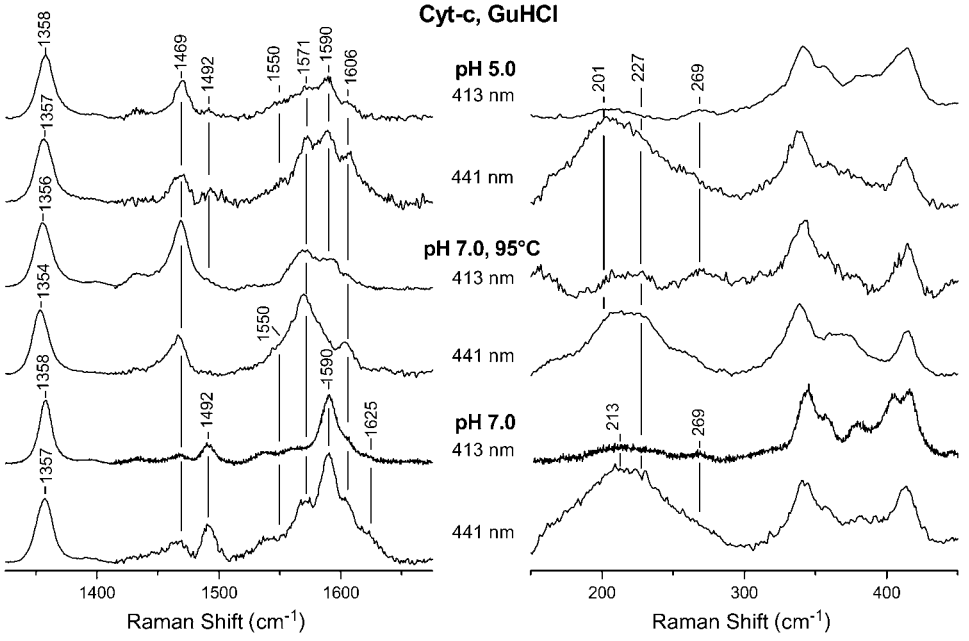

FIGURE 5 RR spectra of ferrous Cyt-*c* in GuHCl (6.3 M) at pH 7.0 and pH 5.0 at ambient temperature, and at pH 7.0 at 95°C measured in the marker band (*left panel*) and low-frequency region (*right panel*), using 413- and 441-nm excitations. The laser power at the sample was 10 mW. The spectra were recorded with a spectral resolution of 4 cm^{-1}. Integration times vary between 6 s (pH 7.0, 413-nm excitation) and 100 min. The 1415–1675 cm^{-1} and 150–500 cm^{-1} regions have been expanded by a factor of five and seven, respectively.

bond and the displacement of the peptide segment 80–85 out of the heme pocket. To generate the bis-His-coordinated 6cLS species the peptide segment 30(20)–49 has to swing toward the heme crevice to bring His-33 (His-26) in bonding distance to the heme. For ferric Cyt-*c*, these reorganizations of the polypeptide chain are not associated with variations in secondary structure as judged from circular dichroism and infrared spectroscopic measurements (13,45,46). This conclusion most likely holds also for ferrous Cyt bound to SDS or DOPG taking into account the higher protein stability as compared to ferric Cyt-*c*. These nonnative states of ferrous and ferric Cyt-*c* for which the secondary structure is largely preserved are denoted as B2 states (13). The conversion between these B2 states and the native state, denoted as B1, has also been observed for Cyt-*c* immobilized on (coated) electrodes and shown to be coupled to the interfacial redox process (47,48).

The transition to the states B2 can be induced by electrostatic or hydrophobic interactions. Strong electrostatic fields which are present upon Cyt-*c* binding to anionic surfaces (e.g., SDS micelles, DOPG vesicles) may induce dipoles, align dipoles, and shift protonation equilibria in the interior of a protein (49), specifically in the vicinity of the interaction domain, and thus may substantially perturb the hydrogen-bond network. In Cyt-*c*, these distortions may lead to a destabilization of the Fe-Met-80 bond as the first step of the B1 → B2 transition. In fact, the portion of the B2 state of ferric Cyt-*c* immobilized on electrodes has been shown to increase with the electric field strength (50). On the other hand, the formation of B2 induced by interactions with hydrophobic surfaces is most likely initiated by an attack on the hydrophobic peptide segment 80–85, which leads to a weakening and finally to the rupture of the Fe-Met-80 bond. This mechanism may represent a crucial step in the unfolding process of Cyt-*c* induced by denaturants in both ferrous and ferric states.

However, in contrast to the nonnative B2 states, a substantially larger degree of protein unfolding is expected to occur for Cyt-*c* in GuHCl at low pH or high temperatures, both in the ferric and in the ferrous form (13). Unlike the immobilization on hydrophobic surfaces (e.g., electrodes coated with self-assembled monolayers of alkanethiols (51)), the interactions are not restricted to the protein surface around the exposed heme edge such that GuHCl-induced unfolding of the polypeptide chain may take place at quite different sites of the protein. These Cyt-*c* species are, therefore, denoted as U-states to indicate the unfolded protein structure even though the heme configurations are the same as in the corresponding species of the B2 state (13). The UV-Vis and RR spectral parameters of all nonnative ferrous Cyt-*c* species are listed in Table 1. Table 2 summarizes under which conditions the various native and nonnative states are formed.

*Quantitative distributions of the unfolded ferrous Cyt-*c *species bound to SDS and DOPG*

Complexes of ferrous Cyt-*c* with SDS and DOPG were prepared at different protein/amphiphile ratios. The RR spectra in the marker band region obtained from these samples were subjected to a component analysis in which complete spectra, which include all the individual components, are fitted to the experimental spectra (30). This analysis allows a quantitative determination of the relative concentration of the individual B1 and B2 states as described previously (13).

Fig. 6 shows the relative concentrations of the various ferrous Cyt-*c* species as a function of the SDS concentration. Increasing the SDS concentration to the cmc (~2 mM) results in the formation of up to ~80% B2[5cHS(1)] at the expense of the native B1 state. A further increase of the SDS concentration leads to an almost complete conversion of B2. Whereas the B2[5cHS(1)] concentration remains at ~80% also for higher SDS concentrations, the second 5cHS species, B2[5cHS(2)], and the bis-His ligated B2[6cLS] species reach relative concentrations of ~10% each. The conversion of B1 to the nonnative species is thus complete at the cmc of SDS, but unlike to ferric Cyt-*c* (52), increasing the SDS concentration above the cmc does not result in significant changes in the relative concentration of the B2 states.

TABLE 1 Spectral properties of the four nonnative (B2) and the native (B1) heme configurations of ferrous Cyt-*c*

Spectral properties	B2* 5cHS(1) -/His. . .H	B2* 5cHS(2) -/His	B2 5cHS(3) -/His$^-$	B2* 6cLS His/His	B1 6cLS Met/His
RR† (cm^{-1})					
ν(Fe-Im)‡	227	201	251	–	–
ν_4	1353.7	1359.9	1355	1360.0	1361.1
ν_2	1572.7	1569.6	1571	1592.0	1591.2
ν_{10}	1606.3	1604.7	1606	n.d.	1621.0
UV-Vis§ (nm)					
Soret band	433	420	437	417	415
Q band	565		586	520, 550	520, 550

*Spectral parameters are the same as for the corresponding U-states.

†Band frequencies for the marker bands of B2[5cHS(1)], B2[5cHS(2)], B2[6cLS], and B1[6cLS] have been determined previously (13).

‡The predominant form is reported.

§Band maxima determined from the D^2 spectra.

TABLE 2 Formation of the various nonnative (B2) and native (B1) states of ferrous Cyt-*c* under different conditions

	B2 5cHS(1) -/His. . .H	B2 5cHS(2) -/His	B2 5cHS(3) -/His$^-$	B2 6cLS His/His	B1 6cLS Met/His
Exp. Conditions					
pH 7.0					X
SDS pH 7.0	X	X			
DeTAB alk. pH	X	X	X	X	
GuHCl pH 7.0	X			X	
GuHCl pH 7.0, 95°C	X	X		X	
GuHCl pH 5.0	X	X		X	
DOPG pH 7.0	X	X		X	X

Fig. 7 shows the relative concentrations of the B1 and B2 states as a function of the L/P ratio. At high DOPG/Cyt-*c* ratios, Cyt-*c* exists exclusively in the nonnative B2[5cHS(1)] and B2[5cHS(2)] states with relative concentrations of ~35% and 55%, respectively. Lowering the L/P ratio by maintaining the Cyt-*c* concentration constant and decreasing the DOPG concentration, results in an increase of the relative concentration of the native B1 state at the expense of the HS states. For an L/P ratio of ~30:1, already ~50% of the bound Cyt-*c* is found in the B1 state. This behavior is quite different compared to ferric Cyt-*c*, which remains fully in the B2 states down to L/P ratios of ~20:1 and undergoes a much steeper transition to the native form upon further lowering the L/P ratio (53). This difference can be rationalized in terms of the dependence of the local electrostatic field on the surface coverage. Upon increasing the amount of bound protein per phospholipid vesicle, the surface potential decreases due to neutralization of the anionic charges on the lipid headgroups by the cationic protein. Such a dependence of the electrostatic interactions on the amphiphile/protein ratio does not exist in the case of SDS above the cmc. In this regime, the number of SDS micelles bound to Cyt-*c* is ~1 and independent of the number of micelles in solution (52).

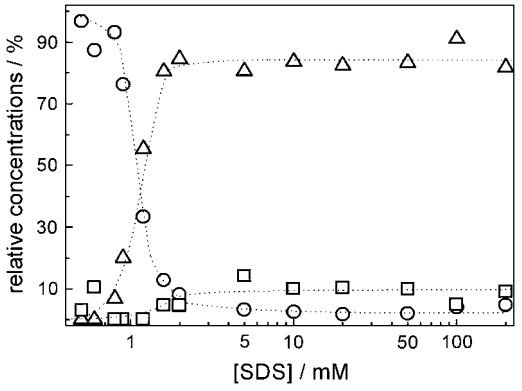

FIGURE 6 Relative concentrations of the ferrous Cyt-*c* species in the presence of SDS. The data were determined from the component analysis of the RR spectra measured at ambient temperature in 50 mM phosphate buffer (pH 7.0) as a function of the SDS concentration. The protein concentration was 15 μM. Further details are given in the text. The different species are represented by the following symbols: (○) B1[6cLS], (Δ) B2[5cHS(1)], and (□) B2[5cHS(2)]. The data points for B2[6cLS], which exhibits a largely constant and small relative concentration (<10%) in the entire SDS concentration range, have been omitted for the sake of clarity of the representation. In some RR spectra minor concentrations (<5%) of ferric B1[6cLS] and B2[6cLS] were found. These contributions were added to those of the ferrous B1[6cLS] and B2[6cLS] states, respectively. The dotted lines are to guide the eye.

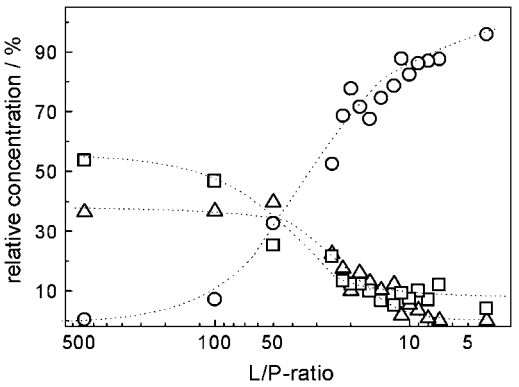

FIGURE 7 Relative concentrations of the ferrous Cyt-*c* species in complexes with DOPG vesicles. The data were determined from the component analysis of the RR spectra measured at ambient temperature in 5 mM HEPES/1 mM EDTA buffer (pH 7.0) as a function of the L/P ratio. The protein concentration was 10 μM. Further details are given in the text. The different Cyt-*c* species are represented by the following symbols: (○) B1[6cLS], (Δ) B2[5cHS(1)], and (□) B2[5cHS(2)]. The data points for B2[6cLS], which gradually decreases from 10% at L/P = 500 to 0% at L/P = 20, have been omitted for the sake of clarity of the representation. In some RR spectra, minor concentrations of ferric B1[6cLS] and B2[6cLS] were found. These contributions were added to those of the ferrous B1[6cLS] and B2[6cLS] states, respectively. The dotted lines are to guide the eye.

Structural perturbations on the proximal side of the heme

A common feature of all nonnative states of ferrous Cyt-*c* is the loss of the distal Met ligand such that this coordination site remains vacant leading to various 5cHS configurations, or it is occupied by a His residue (His-33 or His-26) giving rise to a 6cLS form. The 5cHS forms, which represent the dominant species, differ mainly with regard to the interactions of the proximal His-18 ligand. In neutral or acid solutions two spectroscopically different states of His-18, i.e., a nonhydrogen-bonded and a strongly hydrogen-bonded His are observed, whereas at alkaline pH a species with a deprotonated His ligand is present.

In ferric Cyt-*c*, the contributions of the B2 substates and, among them, specifically the HS forms, increase at the expense of the B1 state when the electric field strength is increased (13,50,52,53). Thus, the concentration ratios between the B2 substates and the native state B1 or between the 5cHS and 6cLS species of the ferric B2 state ([HS]/[LS]) determined previously (52,53) can be taken as a measure for the strength of the local electric field experienced by the bound protein in electrostatic complexes. Correspondingly, electrostatic interactions are concluded to be stronger for Cyt-*c* bound to

SDS micelles ([HS]/[LS] $\cong$ 1.2) compared to DOPG vesicles at L/P = 100 ([HS]/[LS] $\cong$ 0.55). This conclusion is consistent with the results for ferrous Cyt-*c* obtained in this work. For DOPG vesicles at L/P = 100, we still observe a residual contribution of the native state B1 ($\sim$10%) implying that the electrostatic field is not sufficiently strong for a complete shift of the conformational equilibrium toward the B2 states. For ferric Cyt-*c* no native state could be detected under these conditions, reflecting the intrinsically higher stability of the heme pocket and, specifically, of the Fe-Met bond in the ferrous state (13,16). However, upon complexation with SDS micelles, ferrous Cyt-*c* also exists exclusively in the state B2, confirming the view that local electrostatic fields are larger at these micelles than at DOPG vesicles.

Moreover, the distribution between the B2[5cHS(1)] and B2[5cHS(2)] forms of ferrous Cyt-*c* is also different in complexes with SDS micelles and DOPG vesicles and, thus, appears to be electric-field dependent. Figs. 6 and 7 show a distinctly higher contribution of B2[5cHS(1)] in complexes with SDS micelles ($\sim$80%) than with DOPG vesicles ($\sim$40%), which is in qualitative agreement with the relative intensities of the ν(Fe-Im) modes measured for both samples on the basis of a band-fitting analysis of the low-frequency region (Supplementary Material). It appears that the somewhat stronger electrostatic interactions with SDS micelles stabilize the polar hydrogen-bonded His-18, which carries a partial negative charge on the imidazole ring.

In GuHCl at pH 7.0 and ambient temperature, the bis-His ligated U[6cLS] state of ferrous Cyt-*c* is the prevailing state and the only high spin species refers to the U[5cHS(1)] form. When the polypeptide chain unfolding is increased, either through raising the temperature to 95°C or lowering the pH to 5.0, the contribution of U[6cLS] decreases and the U[5cHS(2)] state grows in. We, therefore, conclude that the loss of the hydrogen-bond of the His-18 ligand in U[5cHS(2)] results from a structural rearrangement on the proximal side of the heme. These results are of relevance for understanding the unfolding mechanism of ferrous Cyt-*c*. Since the U[6cLS] and U[5cHS(1)] states are converted to U[5cHS(2)] only under ''harsh'' denaturing conditions (i.e., GuHCl at low pH or high temperature), we conclude that unfolding of the protein is initiated by the rupture of the Fe-Met-80 bond and first restricted to the distal side of the heme pocket. Subsequently, also the proximal heme side is attacked. These two steps may correspond to the ''ligand exchange'' and ''nascent'' phase that have been shown to constitute the biphasic folding process of ferric Cyt-*c* and proposed to hold for ferrous Cyt-*c* as well (15).

On the other hand, the results here also imply that, contrary to previous suggestions (13), the conformational changes in the heme pocket of the ferrous B2 states are not restricted to the vicinity of the Met-80 ligand but may also extend to the proximal heme side as reflected by the contributions of the B2[5cHS(2)] state in complexes with SDS micelles and DOPG vesicles.

SUPPLEMENTARY MATERIAL

An online supplement to this article can be found by visiting BJ Online at http://www.biophysj.org.

This work was funded by grants from the Italian Ministry of Education, Universities, and Research (COFIN 2001031798) and the Università di Firenze (ex 60%) to G.S. and from the Deutsche Forschungsgemeinschaft (Sfb 498, A8) to P.H.

REFERENCES

1. Scott, R. A., and A. G. Mauk. 1995. Cytochrome *c*—A Multidisciplinary Approach. University Science Books, Sausalito, CA.
2. Liu, X., C. N. Kim, J. Yang, R. Jemmerson, and X. Wang. 1996. Induction of apoptotic program in cell-free extracts: requirement for DATP and cytochrome *c*. *Cell*. 86:147–157.
3. Kluck, R. M., L. M. Ellerby, H. M. Ellerby, S. Naiem, M. P. Yaffe, E. Margoliash, D. Bredesen, A. G. Mauk, F. Sherman, and D. D. Newmeyer. 2000. Determinants of cytochrome *c* pro-apoptotic activity. The role of lysine 72 trimethylation. *J. Biol. Chem.* 275:16127–16133.
4. Feng, Y., H. Roder, S. W. Englander, A. J. Wand, and D. L. Di Stefano. 1989. Proton resonance assignments of horse ferricytochrome *c*. *Biochemistry*. 28:195–203.
5. Feng, Y., H. Roder, and S. W. Englander. 1990. Assignment of paramagnetically shifted resonances in the ^{1}H NMR spectrum of horse ferricytochrome *c*. *Biophys. J.* 57:15–22.
6. Bushnell, G. W., G. V. Louie, and G. D. Brayer. 1990. High resolution three-dimensional structure of horse heart cytochrome *c*. *J. Mol. Biol.* 214:585–595.
7. Englander, S. W. 2000. Protein folding intermediates and pathways studied by hydrogen exchange. *Annu. Rev. Biophys. Biomol. Struct.* 29: 213–238.
8. Freire, E. 1995. Thermodynamics of partly folded intermediates in proteins. *Annu. Rev. Biophys. Biomol. Struct.* 24:141–165.
9. Takahashi, S., S.-R. Yeh, T. K. Das, C.-K. Chan, D. S. Gottfried, and D. L. Rousseau. 1997. Folding of cytochrome *c* initiated by submillisecond mixing. *Nat. Struct. Biol.* 4:44–50.
10. Yeh, S.-R., S. Takahashi, B. Fan, and D. L. Rousseau. 1997. Ligand exchange during cytochrome *c* folding. *Nat. Struct. Biol.* 4:51–56.
11. Yeh, S.-R., and D. L. Rousseau. 1998. Folding intermediates in cytochrome *c*. *Nat. Struct. Biol.* 5:222–228.
12. Russell, B. S., and K. L. Bren. 2002. Denaturant dependence of equilibrium unfolding intermediates and denatured state structure of horse ferricytochrome *c*. *J. Biol. Inorg. Chem.* 7:909–916.
13. Oellerich, S., H. Wackerbarth, and P. Hildebrandt. 2002. Spectroscopic characterization of nonnative conformational states of cytochrome *c*. *J. Phys. Chem. Part B*. 106:6566–6580.
14. Chevance, S., E. Le Rumeur, J. D. de Certaines, G. Simonneaux, and A. Bondon. 2003. ^{1}H NMR structural characterization of the cytochrome *c* modifications in a micellar environment. *Biochemistry*. 42: 15342–15351.
15. Yeh, S.-R., S.-W. Han, and D. L. Rousseau. 1998. Cytochrome *c* folding and unfolding: a biphasic mechanism. *Acc. Chem. Res.* 31:727–736.
16. Tezcan, F. A., J. R. Winkler, and H. B. Gray. 1998. Effects of ligation and folding on reduction potentials of heme proteins. *J. Am. Chem. Soc.* 120:13383–13388.
17. Bhuyan, A. K., and R. Kumar. 2002. Kinetic barriers to the folding of horse cytochrome *c* in the reduced state. *Biochemistry*. 41:12821–12834.
18. Nishida, S., T. Nada, and M. Terazima. 2005. Hydrogen-bonding dynamics during protein folding of reduced cytochrome *c*: temperature and denaturant concentration dependence. *Biophys. J.* 89:2004–2010.
19. Varhac, R., and M. Antalík. 2004. Determination of the pK for the acid-induced denaturation of ferrocytochrome *c*. *Biochemistry*. 43: 3564–3569.

20. Chen, E., R. A. Goldbeck, and D. S. Kliger. 2003. Earliest events in protein folding: submicrosecond secondary structure formation in reduced cytochrome *c*. *J. Phys. Chem. A.* 107:8149–8155.
21. Wang, W., X. Ye, A. A. Demidov, F. Rosca, T. Sjodin, W. Cao, M. Sheeran, and P. M. Champion. 2000. Femtosecond multicolor pump-probe spectroscopy of ferrous cytochrome *c*. *J. Phys. Chem. B*. 104: 10789–10801.
22. Cianetti, S., M. Négrerie, M. H. Vos, J.-L. Martin, and S. G. Kruglik. 2004. Photodissociation of heme distal methionine in ferrous cytochrome *c* revealed by subpicosecond time-resolved resonance Raman spectroscopy. *J. Am. Chem. Soc.* 126:13932–13933.
23. Bhuyan, A. K., and J. B. Udgaonkar. 2001. Folding of horse cytochrome *c* in the reduced state. *J. Mol. Biol.* 312:1135–1160.
24. Varhac, R., M. Antalík, and M. Bánó. 2004. Effect of temperature and guanidine hydrochloride on ferrocytochrome *c* at neutral pH. *J. Biol. Inorg. Chem.* 9:12–22.
25. Hagen, S., R. F. Latypov, D. A. Olgikh, and H. Oder. 2002. Rapid intrachain binding of histidine-26 and histidine-33 to heme in unfolded ferrocytochrome *c*. *Biochemistry.* 41:1372–1380.
26. Telford, J. R., F. A. Tezcan, H. B. Gray, and J. R. Winkler. 1999. Role of ligand substitution in ferrocytochrome *c* folding. *Biochemistry.* 38: 1944–1949.
27. Yoshimura, T. A. 1988. Change in the heme stereochemistry of cytochrome upon addition of sodium dodecyl sulfate. Electron paramagnetic resonance and electronic absorption spectral study. *Arch. Biochem. Biophys.* 264:450–461.
28. Hildebrandt, P., and M. Stockburger. 1989. Cytochrome *c* at charged interfaces. 1. Conformational and redox equilibria at the electrode/electrolyte interface probed by surface-enhanced resonance Raman spectroscopy. *Biochemistry.* 28:6710–6721.
29. Wang, J.-S., and H. E. Van Wart. 1989. Resonance Raman characterization of the heme *c* group in *N*-acetyl microperoxidase-8: a thermal intermediate spin-high spin state mixture. *J. Phys. Chem.* 93:7925–7931.
30. Döpner, S., P. Hildebrandt, A. G. Mauk, H. Lenk, and W. Stempfle. 1996. Analysis of vibrational spectra of multicomponent systems. Application to pH-dependent resonance Raman spectra of ferricytochrome *c*. *Spectrochimica Acta A.* 52:573–584.
31. Margoliash, E., and N. Frohwirt. 1959. Spectrum of horse-heart cytochrome *c*. *Biochem. J.* 71:570–572.
32. Andrew, C. R., E. L. Green, D. M. Lawson, and R. R. Eady. 2001. Resonance Raman studies of cytochrome *c′* support the binding of NO and CO to opposite sides of the heme: implications for ligand discrimination in heme-based sensor. *Biochemistry.* 40:4115–4122.
33. Othman, S., A. Le Lirzin, and A. Desbois. 1993. A heme *c*-peptide model system for the resonance Raman study of *c*-type cytochromes: characterization of the solvent-dependence of peptide-histidine-heme interactions. *Biochemistry.* 32:9781–9791.
34. Marques, H. M., and C. B. Perry. 1999. Hemepeptide models for hemoproteins: the behavior of *N*-acetylmicroperoxidase-11 in aqueous solution. *J. Inorg. Biochem.* 75:281–291.
35. Vashi, P. R., and H. M. Marques. 2004. The coordination of imidazole and substituted pyridines by the hemeoctapeptide *N*-acetyl-ferromicroperoxidase-8 (Fe^{II}NAcMP8). *J. Inorg. Biochem.* 98:1471–1482.
36. Spiro, T. G., and X.-Y. Li. 1988. Resonance Raman Spectroscopy of Metalloporphyrins, Vol. 3. T. G. Spiro, editor. John Wiley & Sons, New York.
37. Stein, P., and T. G. Spiro. 1980. Hydrogen-bond and deprotonation effects on the resonance Raman iron-imidazole mode in deoxyhemoglobin models: implication for hemoglobin cooperativity. *J. Am. Chem. Soc.* 102:7795–7797.
38. Hori, H., and T. Kitagawa. 1980. Iron-ligand stretching band in the resonance Raman spectra of ferrous iron porphyrin derivatives. Importance as a probe for quaternary structure of hemoglobin. *J. Am. Chem. Soc.* 102:3608–3613.
39. Hu, S., I. K. Morris, J. P. Singh, K. M. Smith, and T. G. Spiro. 1993. Complete assignment of cytochrome *c* resonance Raman spectra via enzymatic reconstitution with isotopically labeled hemes. *J. Am. Chem. Soc.* 115:12446–12458.
40. Santoni, E., S. Scatragli, F. Sinibaldi, L. Fiorucci, R. Santucci, and G. Smulevich. 2004. A model for the misfolded bis-His intermediate of cytochrome *c*: the 1-56 N-fragment. *J. Inorg. Biochem.* 98:1067–1077.
41. Othman, S., P. Richard, A. Vermeglio, and A. Desbois. 1996. Evidence for a proximal histidine-protein interaction in the structure of cytochromes *c′* in solution: a resonance Raman study. *Biochemistry.* 35: 9224–9234.
42. Smulevich, G., A. Feis, and B. D. Howes. 2005. Fifteen years of Raman spectroscopy of engineered heme containing peroxidases: what have we learned? *Acc. Chem. Res.* 38:433–440.
43. Berghuis, A. M., and G. D. Brayer. 1992. Oxidation state-dependent conformational changes in cytochrome *c*. *J. Mol. Biol.* 223:959–976.
44. Samuni, U., Y. Ouellet, M. Guertin, J. M. Friedman, and S. R. Yeh. 2004. The absence of proximal strain in the truncated hemoglobins from mycobacterium tuberculosis. *J. Am. Chem. Soc.* 126:2682–2683.
45 Muga, A., H. H. Mantsch, and W. K. Surewicz. 1991. Membrane binding induces destabilization of cytochrome *c* structure. *Biochemistry.* 30:7219–7224.
46. Heimburg, T., and D. Marsh. 1993. Investigation of secondary and tertiary structural changes of cytochrome *c* in complexes with anionic lipids using amide hydrogen exchange measurements: an FTIR study. *Biophys. J.* 65:2408–2417.
47. Murgida, D. H., and P. Hildebrandt. 2004. Electron transfer processes of cytochrome *c* at interfaces. New insights by surface-enhanced resonance Raman spectroscopy. *Acc. Chem. Res.* 37:854–861.
48. Murgida, D. H., and P. Hildebrandt. 2005. Redox and redox-coupled processes of heme proteins and enzymes at electrochemical interfaces. *Phys. Chem. Chem. Phys.* 7:3773–3784.
49. Neumann, E. 1986. Chemical electric field effects in biological macromolecules. *Prog. Biophys. Mol. Biol.* 47:197–231.
50. Murgida, D. H., and P. Hildebrandt. 2001. Heterogeneous electron transfer of cytochrome *c* on coated silver electrodes. Electric field effects on structure and redox potential. *J. Phys. Chem. B.* 105:1578–1586.
51. Rivas, L., D. H. Murgida, and P. Hildebrandt. 2002. Conformational and redox equilibria and dynamics of cytochrome *c* immobilized on electrodes via hydrophobic interactions. *J. Phys. Chem. B.* 106:4823–4830.
52. Oellerich, S., H. Wackerbarth, and P. Hildebrandt. 2003. Conformational equilibria and dynamics of cytochrome *c* induced by binding of sodium dodecyl sulfate monomers and micelles. *Eur. Biophys. J.* 32: 599–613.
53. Oellerich, S., S. Lecomte, M. Paternostre, T. Heimburg, and P. Hildebrandt. 2004. Peripheral and integral binding of cytochrome *c* to phospholipids vesicles. *J. Phys. Chem. B.* 108:3871–3878.